This article has been accepted for publication in a future issue of this journal, but has not been fully edited. Content may change prior to final publication. Citation information: DOI 10.1109/JSTQE.2015.2413955, IEEE Journal of Selected Topics in Quantum Electronics

Dynamics of Normal and Reverse Polarization Switching in 1550nm-VCSELs under Single and Double Optical Injection

M. Salvide, M. S. Torre, I. D. Henning, M. J. Adams and A. Hurtado

***Abstract*—Polarization switching (PS) in 1550nm-VCSELs under single and double pulsed polarized optical injection is investigated experimentally and in theory. 'Normal' and 'reverse' PS were achieved, respectively, when the device was subject to single and double optical injection. Speed operation enhancement is observed for 'reverse' PS under double polarized optical injection. Also, the minimum injection power requirements for both 'normal' and 'reverse' PS have been analyzed showing significant differences for the two investigated cases. Furthermore, we have also investigated numerically the influence of important system parameters, such as the normalized bias current, the injection field strength and the linewidth enhancement factor in the optimal operation conditions for both types of PS. Overall good agreement between theory and experiments is found.**

***Index Terms*—Vertical-cavity surface emitting lasers (VCSEL), optical injection, polarization switching.**

I. Introduction

Vertical-cavity surface emitting lasers (VCSELs) exhibit very attractive advantages in comparison to edge-emitting lasers. These include amongst others reduced threshold current, single longitudinal mode operation, circular output beam profile, high bandwidth modulation, reduced manufacturing costs, ease to integrate in 2-D arrays, and wafer scale integration (for a review see [1] for instance). Such features make VCSELs ideal devices for use in a rich variety of advanced applications in present and future optical systems and networks [2][3].

A very significant aspect of VCSELs that has attracted much attention in recent years refers to their specific polarization properties. For instance, VCSELs can undergo polarization instabilities that can produce polarization switching (PS) between the two orthogonal polarizations of the fundamental transverse mode of a VCSEL [4-14]. PS can be obtained for instance by varying the device's operation conditions, including the control of the applied bias current or temperature [4-6] or using different techniques such as optical feedback [7][8] or external optical injection (OI) [9-14].

OI is indeed a commonly used technique to affect and investigate the VCSEL's polarization characteristics. Different phenomena such as PS, injection locking, bistability and a rich variety of additional nonlinear responses can be induced in VCSELs under the injection of external light (for a review see [1]). A simple way to induce PS in a VCSEL is to inject an optical signal whose polarization is orthogonal to that of the VCSEL's lasing mode, a situation usually known as orthogonally-polarized optical injection. Additionally, the achievement of PS in VCSELs has also been recently reported under different cases of polarized optical injection, including orthogonal [9-11], parallel [12] and arbitrary polarized injection [13][14].

In recent years, PS in long wavelength VCSELs, emitting at the important telecom wavelength of 1550nm, has undergone considerable theoretical and experimental investigation [15-18]. PS and Polarization Bistability (PB) have been observed in single-transverse mode VCSELs subject to orthogonally-polarized optical injection when controlling the injected optical power and the initial detuning between the wavelengths of the injected signal and that of the VCSEL [17][18]. Also, in view of the potential uses of PS and PB in different applications, the analysis of several important characteristics of PS in VCSELs, such as the hysteresis cycle width [19-24], operation speed [25-31] and minimal power requirements for PS [15] has started to attract the attention of the research community.

Fast operation speeds (of several GHz [33]) and low input power requirements (of only a few µWs [15]) have been reported for PS induced by optical injection in VCSELs, thus offering potential for all-optical signal-processing applications for use in future optical networks. For instance, an all-optical inverter has been recently reported using the PS in a 1550nm-VCSEL under single optical injection (SOI) with orthogonal polarization [29]. Moreover, speed operation enhancement has been predicted for a VCSEL-inverter under double optical

Manuscript received November 17, 2014. This work was supported in part by the European Union Seventh Framework Programme (FP7/2007-2013) under grant agreement n° PIOF-GA-2010-273822.

A. Hurtado is with the Institute of Photonics, University of Strathclyde, Wolfson Centre, 106 Rottenrow East, Glasgow, G4 0NW, UK and with the University of Essex, Wivenhoe Park, Colchester, CO4 3SQ, UK (phone: +44(0)141 390 4668; e-mail: antonio.hurtado@strath.ac.uk).

M. Salvide and M.S. Torre are with the Instituto de Física "Arroyo Seco" IFAS-CIFICEN-CONICET, Pinto 399 (7000) Tandil, Provincia de Buenos Aires. Argentina.

I.D. Henning and M.J. Adams are with the School of Computer Science and Electronic Engineering, University of Essex, Wivenhoe Park, Colchester, CO4 3SQ, United Kingdom

This article has been accepted for publication in a future issue of this journal, but has not been fully edited. Content may change prior to final publication. Citation information: DOI 10.1109/JSTQE.2015.2413955, IEEE Journal of Selected Topics in Quantum Electronics

injection (DOI) [30]. Other uses of PS in VCSELs include optical buffer memory [25][26], flip-flop elements [27][28], optical signal regeneration [31], optical logic gates [34][35], novel photonic neurons [36][37], etc.

However, to assess the potential of PS in 1550nm-VCSELs for their use in real systems it is necessary to investigate the response when time-varying signals (similar to data streams) are injected into the device. Therefore, in this work we have analyzed experimentally and in theory the effect of pulsed OI in the PS induced in a 1550nm-VCSEL. Two different cases have been analyzed: SOI and DOI, producing respectively 'normal PS' (from parallel to orthogonal polarization) and 'reverse PS' (from orthogonal to parallel polarization) at the VCSEL's output. We confirm experimentally the theoretical prediction that a faster response is obtained when the device is subject to DOI [30]. Furthermore, we have also analyzed minimum injection strength to achieve PS in both injection cases considered for different important system parameters. Overall good agreement is found between theory and experiments.

Our paper is organized as follows. Section II introduces the concepts of normal and reverse polarization switching. Section III presents the experimental setup used in this work. Section IV presents an extended version of the Spin Flip Model (SFM) model which was used to simulate the polarization-resolved temporal dynamics of a VCSEL subject to single and double pulsed injection. In Section V we present the experimental and theoretical results showing overall good agreement between the numerical and experimental findings. Finally, Section V includes the discussion of the results and conclusions of this work.

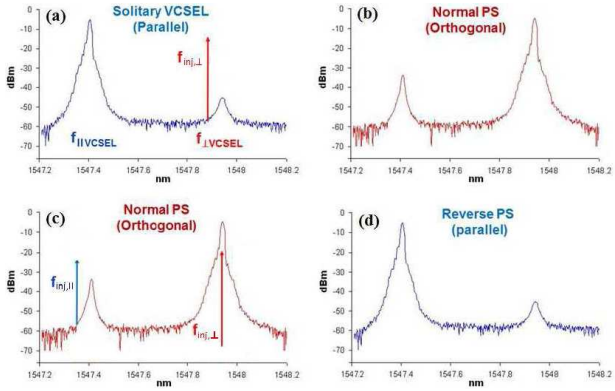

Fig. 1. (color online) Optical spectrum of the 1550nm-VCSEL operating (a) alone (in blue) and (b) subject to SOI producing 'normal PS' (in red). Optical spectrum of the 1550nm-VCSEL subject to DOI (c) before (in red) and (d) after (in blue) the achievement of 'reverse PS'.

II. Normal and Reverse PS (SOI & DOI)

Fig. 1(a) plots the optical spectrum of the free-running VCSEL used in this work showing two modes (a lasing and a subsidiary mode). These correspond respectively to the two orthogonal polarizations of the VCSEL's fundamental transverse mode. Throughout this work we associate "parallel or *y*" ("orthogonal or *x*") polarization with the polarization of the lasing (subsidiary) mode of the VCSEL.

Fig. 1(b) illustrates graphically the achievement of 'normal PS' when the VCSEL is subject to SOI. An orthogonally-polarized optical signal (indicated by the red arrow in fig. 1(a)) is injected into the orthogonal polarization mode of the VCSEL. The latter locks to the externally-injected signal whereas the parallel polarization mode is suppressed. As a result the VCSEL's polarization switches and the device emits now light with orthogonal polarization [14].

The second scenario analyzed refers to the case when the device is subject to DOI. Now, a constant orthogonally-polarized optical signal (indicated by the red arrow in fig. 1(c)) is initially injected into the VCSEL producing 'normal PS'. In this situation, a second parallel-polarized optical signal (indicated by the blue arrow in fig. 1(c)) is injected into the VCSEL's parallel polarization mode. The injection of this second signal switches back the polarization of the VCSEL from orthogonal to parallel producing 'reverse PS' as shown schematically in Fig 1(d).

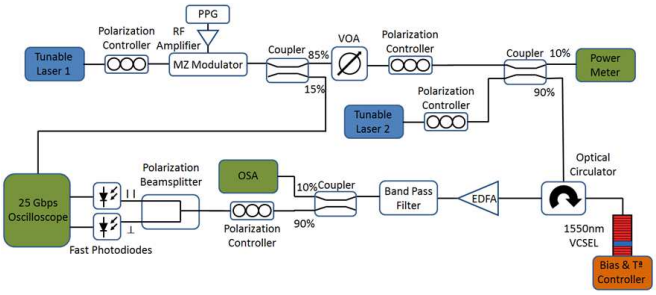

Fig. 2. (Color online) (a) Experimental setup. PPG=Pulse Pattern Generator; VOA=Variable Optical Attenuator; MZ=Mach Zehnder; RF=Radio Frequency; EDFA=Erbium Doped Fibre Amplifier; OSA=Optical Spectrum Analyzer.

III. Experimental Setup

Fig. 2 shows the experimental setup used in this work [14]. An all-optical fibre setup was designed in order to inject polarization controlled light from two tuneable laser sources (TL1 and TL2) into a commercial 1550 nm-VCSEL [38]. The device had a threshold current (I_{th}) of 1.6 mA at 298 K and oscillated in its fundamental transverse mode.

Two different cases of polarized optical injection were analysed in this work, namely SOI and DOI. For the first case, only TL1 was used and it was configured with an orthogonally-polarized output using a polarization controller. For the DOI case, both TL1 and TL2 were simultaneously used, but now their polarizations were respectively set equal to parallel and orthogonal polarizations. The output of TL1 was externally modulated using a 10 Gbps Mach-Zehnder (MZ) modulator and a 12.5 Gbps Pulse Pattern Generator (PPG) to study the injection of time-varying optical signals in the PS induced in the 1550 nm-VCSEL. A variable Optical attenuator (VOA) was also included after TL1 to control the injection strength of this time-varying injected signal. Both lines from TL1 and TL2 were combined using a fibre directional coupler and injected directly into the 1550 nm-VCSEL using an optical circulator. The VCSEL's reflective output was collected and analysed optically using an OSA and electrically with a 25

This article has been accepted for publication in a future issue of this journal, but has not been fully edited. Content may change prior to final publication. Citation information: DOI 10.1109/JSTQE.2015.2413955, IEEE Journal of Selected Topics in Quantum Electronics

Gbps oscilloscope. Also an Erbium Doped Fibre Amplifier (EDFA) and a Tuneable Optical Filter were included before the analysis stage to amplify the collected signal and to eliminate the noise introduced by the amplifier. Finally, the two individual VCSEL polarizations, parallel and orthogonal, were separated using a polarization beam splitter (PBS) and their time dynamics were studied individually and simultaneously using two 12 GHz photodiodes connected to the 25 Gbps sampling scope.

IV. Model

The theoretical model used in this work is based on the SFM [39]. We have extended it to account for the injection of two external fields with polarizations parallel and orthogonal to that of the free–running VCSEL. The rate equations of the extended model are given by:

$$\frac{dE_x}{dt} = \kappa(1+i\alpha)\left[(N-1)E_x + i\,n\,E_y\right] - (\gamma_a + i\,\gamma_p)E_x + \sqrt{\beta_{sp}}\;\xi_x(t) + \kappa_{inj}\;E_{injx}(t)\exp[2\pi i\,\nu_{injx}t] \quad (1)$$

$$\frac{dE_y}{dt} = \kappa(1+i\alpha)\left[(N-1)E_y + i\,n\,E_x\right] + (\gamma_a + i\,\gamma_p)E_y + \sqrt{\beta_{sp}}\;\xi_y(t) + \kappa_{inj}\;E_{injy}(t)\exp[2\pi i\,\nu_{injy}t] \quad (2)$$

$$\frac{dN}{dt} = -\gamma_N\left[N(1+|E_x|^2+|E_y|^2)\right] + \gamma_N\mu - i\gamma_N n(E_yE_x^* - E_xE_y^*) \quad (3)$$

$$\frac{dn}{dt} = -\gamma_s n - \gamma_N n(|E_x|^2+|E_y|^2) - i\gamma_N n(E_yE_x^* - E_xE_y^*) \quad (4)$$

where $E_{x,y}$ are the two linearly polarized (parallel and orthogonal) slowly varying components of the field. N and n are two carrier densities: $N = N^+ + N^-$ and $n = N^+ - N^-$; with N^+ and N^- being carrier populations with opposite spin.

The internal VCSEL parameters are as follows: κ is the field decay rate, γ_N is the decay rate of N, γ_s is the spin-flip relaxation rate, γ_a is the rate of linear dichroism, γ_p is the linear birefringence rate and α is the linewidth enhancement factor. The normalized pumping, μ, is related to the current by [30]:

$$\mu = \frac{I/I_{th} - N_t/N_{th}}{1 - N_t/N_{th}}\left(1 - \frac{\gamma_a}{\kappa}\right) \quad (5)$$

where I and I_{th} are respectively the applied bias current and the threshold current of the VCSEL. N_t and N_{th} correspond respectively to the carrier densities at transparency and at threshold.

The fluctuating nature of the spontaneous emission (with the fraction of spontaneous emission photons that go into the laser mode indicated by β_{sp}) is also included in our calculations since $\xi_x(t)$ and $\xi_y(t)$ are complex Gaussian noise terms of zero mean and time correlation given by $\langle\xi_x(t)\xi^*_y(t')\rangle = 2\delta_{xy}\delta(t-t')$.

The optical injection parameters are: $E_{injx(y)}$ and $\nu_{injx(y)}$ where $E_{injx(y)}$ represents the injected field amplitude in the orthogonal or x- (parallel or y-) polarization whereas $\nu_{injx(y)}$ is the frequency of the orthogonal (or parallel) injected external signal. We must note, however, that all the results are given as a function of the frequency detuning $\Delta\nu_x$ or $\Delta\nu_y$. The latter is defined as the difference between the frequencies of the injected signal in the x- or y-polarization and that of the VCSEL's x- or y-polarization mode: $\Delta\nu_{x(y)} = \nu_{injx(y)} - \nu_{x(y)}$, with $\nu_x = (-\gamma_p + \gamma_a\alpha)/2\pi$ and $\nu_y = (\gamma_p - \gamma_a\alpha)/2\pi$. Here, ν_x *and* ν_y correspond to the relative frequencies of the orthogonal and parallel polarization modes of the VCSEL with respect to a reference frequency $\nu_{ref} = 0$ which is the midpoint between the frequency of each of the modes.

The VCSEL parameters chosen in our simulations were [18] $\gamma_N = 1$ ns^{-1}, $\gamma_p = 192$ rad/ns, $\gamma_a = 2$ rad/ns, $\gamma_s = 1000$ ns^{-1}, $\kappa = 125$ ns^{-1}, $\kappa_{inj} = 35$ ns^{-1}, $\alpha = 2.2$, $\beta_{sp} = 10^{-5}$ns^{-1}. With this choice of parameters the free-running VCSEL emits in the y-linear polarization (parallel polarization mode) and the device did not exhibit current-induced polarization switching for the entire current range analyzed. The coupling coefficient, κ_{inj}, is coincident with the field decay rate because we assume the ideal case of an effectively mode-matched injected input beam. Equations (1) - (4) were simulated using a Platen explicit order 1.5 strong scheme for stochastic differential equations [40].

For the first optical injection scenario analyzed in this work, (SOI), the free-running VCSEL emits in its y-linear polarization and a pulsed optical signal with orthogonal polarization, $E_{injx}(t)$ is injected into the orthogonal polarization mode of the device. This external signal is injected at the frequency of ν_{injx} with an initial frequency detuning of $\Delta\nu_x$ with respect the orthogonal polarization mode of the free-running VCSEL. In this case, there is no injected signal in the parallel mode, i.e. $E_{injy}(t)=0$.

In the second case of analysis, when double optical injection (DOI) is considered, a constant orthogonally-polarized optical signal with E_{injx} and ν_{injx} is firstly injected into the VCSEL at a given detuning with respect to the orthogonal polarization mode of the VCSEL, $\Delta\nu_x$. The injection of this first signal produces 'normal PS' activating the orthogonal polarization at the VCSEL's output. In this situation, a second pulsed optical signal with parallel polarization, $E_{injy}(t)$ is also injected into the device at a frequency of ν_{injy}, and at a frequency detuning equal to $\Delta\nu_y$ (with respect to the VCSEL´s parallel polarization mode). The injection of this second signal switches back the polarization at the VCSEL's output to parallel, thus producing 'reverse' PS.

V. Results and Discussions

The temporal dynamics of the two orthogonal polarizations (parallel and orthogonal) of the 1550 nm-VCSEL are individually and simultaneously analyzed using a fast oscilloscope. Fig. 3 shows the measured time-dynamics at the VCSEL's output under the injection of a time-varying (pulsed) optical signal for the two cases of study SOI (fig. 3(a)) and DOI (fig. 3(b)). The black plot in the upper part of fig. 3 shows the shape and time characteristics of the injected pulsed injected. This is configured with a time duration of 4 ns in both cases and with orthogonal and parallel polarization respectively for the SOI and DOI cases.

This article has been accepted for publication in a future issue of this journal, but has not been fully edited. Content may change prior to final publication. Citation information: DOI 10.1109/JSTQE.2015.2413955, IEEE Journal of Selected Topics in Quantum Electronics

Fig. 3(a) shows the experimentally measured time traces for the parallel (blue) and orthogonal (red) polarizations at the VCSEL's output when the device is subject to SOI. Fig. 3(a) shows the achievement of 'normal' PS, with the activation (suppression) of the orthogonal (parallel) polarization for the whole duration of the injected signal. On the other hand, fig. 3(b) shows now measured time traces for the parallel (blue) and orthogonal (red) polarizations at the VCSEL's output when subject to DOI illustrating the achievement of 'reverse PS'. In this second case, a constant orthogonally polarized signal is injected first into the VCSEL producing 'normal PS'. Therefore, initially the orthogonal (parallel) polarization is active (suppressed) at the device's output. The arrival of the parallel polarized time-varying signal (at a relative time of ≈ 2.7 ns) switches back the polarization from orthogonal to parallel producing 'reverse' PS for the whole time duration (4 ns) of the pulsed injected signal.

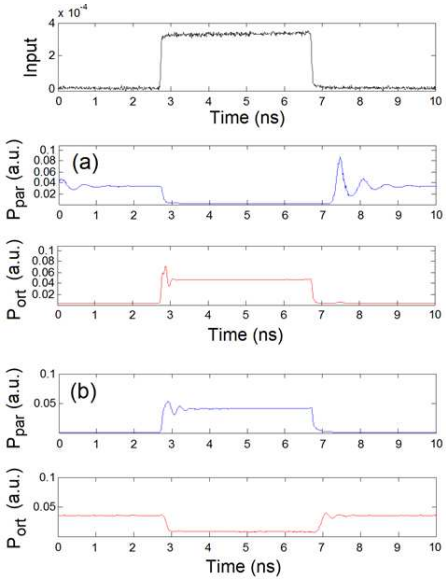

Fig. 3. (Color online) Experimental time traces of the VCSEL's parallel (blue) and orthogonal (red) polarizations under (a) SOI and (b) DOI; The black plot above shows the injected pulsed 4 ns signal with orthogonal (parallel) polarization in the SOI (DOI) case. (a) $\Delta\nu_x$ = -5 GHz. (b) The orthogonally-polarized signal was set with $\Delta\nu_x$ = -5 GHz and constant optical power of 12μW. A detuning of $\Delta\nu_y$ = -5 GHz was set for the pulsed parallel polarized injected signal. In all cases a bias current of 2.4 mA (≈1.5I_{th}) was applied.

Fig. 4 shows calculated time traces, for the parallel and orthogonal polarizations at the output of the 1550nm-VCSEL when subject to SOI and DOI respectively. As in the experimental measurements of fig. 3 we have simulated the optical injection of 4 ns long pulsed signals with either orthogonal or parallel polarization into the VCSEL. Also, similar values of normalized bias current and initial frequency detuning to those used for the experimental plots of fig. 3 were used in the calculated time traces included in fig. 4. The shape and time characteristics of the injected pulsed signals are depicted graphically in the black plot in the upper part of fig. 3. Also, the output power in both polarizations is averaged on a time interval of 0.12 ns using a standard moving average. Fig. 4(a) show results for the SOI case illustrating the achievement of 'normal PS' where switching from parallel to orthogonal polarization is obtained for the whole pulse duration. On the other hand, fig. 4(b) plot calculated results for the DOI case revealing the achievement of 'reverse PS' as in the experimental results depicted in fig. 3(b). For this second case, the initial injection of a constant orthogonally-polarized signal produces 'normal PS'. Note that in fig. 4(b) before the pulse arrival, the orthogonal mode dominates whilst the parallel one is suppressed. Upon the injection of a pulsed optical signal (like that in the black plot of fig. 4) with parallel polarization, 'reverse PS' is achieved and the *y*-polarization (parallel) mode is once again the dominating one for the whole duration of the injected pulse.

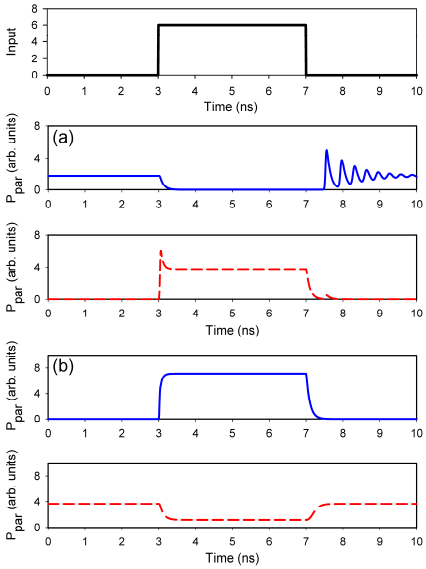

Fig. 4. (Color online) Calculated time traces for the parallel (solid-blue) and orthogonal (dash-red) polarizations at the VCSEL's output under (a) SOI with $\Delta\nu_x$ = -5 GHz and E_{injx} = 6 arb. units and (b) DOI with $\Delta\nu_x$ = -5 GHz and E_{injx} = 6 arb. units and $\Delta\nu_y$ = -5 GHz and E_{injy} = 14 arb. units. The corresponding 4 ns pulse signal injected with either (a) orthogonal or (b) parallel polarization is shown in above black plot. The results were calculated for a value of normalized injection current equal to μ = 2.6 obtained from (5) assuming a value of N_t/N_{th} = 0.7. The output power in both polarizations is averaged on a time interval of 0.1 ns using a standard moving average.

The comparison between figs. 3 and 4 shows good qualitative agreement between experimental and calculated results. In addition to reproduce the achievement of 'normal' and 'reverse' PS in a 1550nm-VCSEL under SOI and DOI, respectively. The model also successfully reproduces the dynamic properties of both types of PS. For the SOI case, after the termination of the injected pulse the recovery of the suppressed polarization (parallel) exhibits large relaxation oscillations which ultimately limit the operation speed of 'normal PS' for optical logic applications [29]. On the other hand a faster recovery time is observed for the suppressed polarization (orthogonal) in the DOI case without the appearance of large amplitude relaxation oscillations. A faster operation speed is therefore observed for 'reverse PS' in the VCSEL under DOI, as theoretically predicted in [30]. The reason for this speed enhancement can be explained from the different transitions experienced by the VCSEL in each case.

This article has been accepted for publication in a future issue of this journal, but has not been fully edited. Content may change prior to final publication. Citation information: DOI 10.1109/JSTQE.2015.2413955, IEEE Journal of Selected Topics in Quantum Electronics

Under SOI the VCSEL switches between an injection locking (orthogonally-polarized injection locking) and its free-running state, thus exhibiting large relaxation oscillations in the recovery of the original polarization (parallel). On the other hand, for the DOI case the VCSEL's response is much faster as the system switches between two injection locking states, from orthogonally-polarized to parallel polarized injection locking, thus eliminating the large relaxation oscillations and therefore allowing a faster recovery speed for the initially active polarization (orthogonal). This result is of importance for future practical uses of VCSELs in polarization sensitive applications as it might allow the development of faster basic all-optical signal processing components. For instance, a faster operation speed has been predicted for a VCSEL-based optical inverter exploiting the Reverse PS under DOI [30]. Also, the faster operation speed for PS in long-wavelength VCSELs could find significant uses in faster all-optical buffer memories and switching elements in future optical networks [25-28].

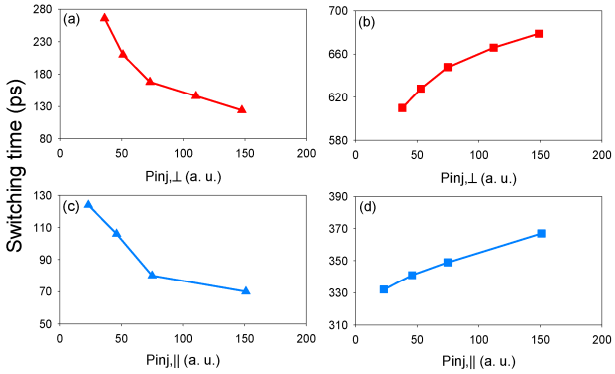

Fig. 5. Experimentally measured switching times vs. input power for the time-varying signal for the SOI case (a & b, red) and DOI case (c & d, blue). Switching times are measured for the inverted polarization in each case of analysis: orthogonal (SOI, a & b) and parallel (DOI, c & d) as it is the one with the slowest time response. Measured times are given for the first switching transition, after the arrival of the pulsed signal (a & c), and the second switching transition, after the removal of the pulsed signal (b & d).

Fig. 5 shows experimentally measured switching times for the 'normal' (figs. 5(a-b)) and 'reverse' PS (figs 5(c-d)) obtained respectively under SOI and DOI. Fig. 5 plots measured switching times for the inverted polarization in each case, parallel (SOI) and orthogonal (DOI), as this has the slowest response times thus limiting the total operation speed of the system. Also, results are given for different injection strength for the injected pulse signal. The measurement conditions used in fig. 5 were as follows: in the SOI case a 4ns-long pulsed signal with orthogonal polarization was injected at a detuning of $\Delta\nu_x$ = -5 GHz. In the DOI case, a CW orthogonally-polarized signal was injected at $\Delta\nu_x$ = -5 GHz with constant power of 12 μW and a 4ns-long pulsed polarized signal was injected at a detuning of $\Delta\nu_y$ = -5 GHz. In all cases a bias current of 2.4 mA (≈1.5I_{th}) was applied to the device. Also, the following criteria were used to measure the switching times in fig. 5: for the first switching transition (upon arrival of the pulsed signal, figs. 5(a) and 5(c)), the measured switching time was the time needed to transit from 10% to 90% of the total amplitude. On the other hand, for the second switching transition (after the removal of the pulsed signal, figs. 5(b) and 5(d)) the switching time was measured as the time needed to reach 90% of the intensity after the disappearance of injected pulsed signal.

Fig. 5 shows that the switching times for the inverted polarization follow similar trends under SOI and DOI. The switching times decreases (increase) with growing injection strength for the first (second) switching transition. However, the results for the DOI case (figs. 5(b) and 5(d)) show a faster operation speed with measured switching times approximately twice as fast as those measured for the SOI case (figs. 5(a) and 5(c)). Furthermore, we must also note here that for comparison purposes, the data measured in figs. 5(c) and 5(d) for the second switching transition did not consider the relaxation oscillations undergone by the system to recover a stable state after the removal of the injected signal. The latter, which are particularly important in the SOI case, impose a further limitation on the time performance of the system for this case [30]. Therefore, as predicted theoretically in [30], a much faster operation response is experimentally demonstrated for the case where the VCSEL is subject to DOI.

This operation speed enhancement under DOI is due to the transition between two different injection locked states experienced by the VCSEL. Injection locking is a technique producing faster carrier dynamics thus yielding a faster modulation bandwidth [41,42]. Therefore a faster switching response with damped recovery relaxation oscillations is observed in the DOI case as the system transits between two different injection locked states. As a result the system recovers faster to a stable state after the injected signal is removed. On the other hand, for the SOI case the system switches between injection-locked and free-running states producing large amplitude inherent relaxation oscillations. The latter significantly increases the recovery time of the system thus limiting its speed of operation.

In this work we were also interested in determining the optimum conditions for the achievement of 'normal' and 'reverse' PS in 1550 nm-VCSELs. Specifically, we are interested in investigating the minimum value of the injected power needed for both cases of PS to occur under SOI and DOI respectively. The latter is defined as the lowest value of P_{inj} (P_{inj}=E^2_{inj}) for which the average intensity of the suppressed polarization (parallel under SOI and orthogonal under DOI) does not exceed 10% of the average intensity of the dominating polarization at the VCSEL's output (orthogonal under SOI and parallel under DOI). For that purpose we have calculated injection locking diagrams plotting the minimum optical power requirements as a function of important system parameters for both cases of study, namely SOI and DOI. In many publications injection locking maps are plotted in the plane of the ratio between the powers injected and emitted by the solitary VCSEL versus frequency detuning, especially when the VCSEL is subject to CW

This article has been accepted for publication in a future issue of this journal, but has not been fully edited. Content may change prior to final publication. Citation information: DOI 10.1109/JSTQE.2015.2413955, IEEE Journal of Selected Topics in Quantum Electronics

optical injection [41][42]. However, in this work, the injection is not constant but time-dependent (pulses of 4ns) which makes it more complicated to compare the injected and emitted power. Also, we analyze results for various applied bias currents yielding different emitted power. Therefore, in this work we decided to plot the injection locking diagrams as a function of the injected optical power. This option also allows easy comparison with experimental data of the points for which minimum optical injection power is needed to achieve 'normal' and 'reverse' PS.

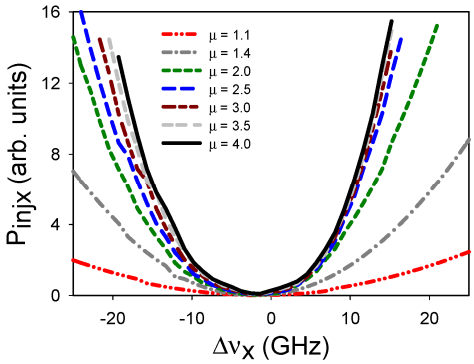

Fig. 6. (color online) Calculated map plotting the minimum injected power for the orthogonally polarized pulsed signals to produce 'normal' PS vs. detuning. Different maps are calculated for several values of normalized injected current bias. The VCSEL is subject to the injection of a 4 ns long pulsed signal with orthogonal polarization.

For the case when the VCSEL is subject to SOI, the calculated map in fig. 6 plots the minimum value of the injected power P_{injx} required for the achievement of 'normal' PS versus the frequency detuning $\Delta\nu_x$ for different values of normalized bias current, μ. Fig. 6 shows that there is a quadratic dependence between P_{injx} and $\Delta\nu_x$, and as consequence, there is an optimal working point in the P_{injx}-$\Delta\nu_x$ plane for which a minimum injected power is required for 'normal PS' to occur. This optimal working point is defined by the vertex of the parabola of P_{injx} as a function of $\Delta\nu_x$. Fig. 6 also shows that this lowest value of the injected power ($P_{injx,min}$) is obtained at nearly zero frequency detuning for all values of normalized bias current considered. In other words, the minimum in the injected power occurs at a frequency very close to the orthogonal polarization of the VCSEL. Fig. 6 also shows that the region where 'normal PS' is obtained shrinks with increasing applied bias current: for a fixed frequency detuning $\Delta\nu_x$, the injected power strength (P_{injx}) required to produce 'normal PS' grows as the applied bias current is increased. These results obtained for time-varying optical injection are in good agreement with previous studies of 'normal PS' in single-transverse mode 1550 nm-VCSELs subject to constant orthogonally-polarized injection [15]. On the contrary, in a recent work [43] using a short-wavelength multiple transverse mode VCSEL, the injected minimum power required to obtain PS decreased with increasing bias current. This different response can be explained as being due to the important role played by the higher-order transverse mode in the device used in [43].

Moreover, the calculated results in fig. 6 are in good agreement with the corresponding experimental map of Fig. 7(a). Fig. 7(a) plots results for two different values of bias current applied to the 1550 nm-VCSEL, namely 2.4 mA (1.5 I_{th}) and 4 mA (2.5 I_{th}). As in the calculated maps of fig. 6, the measured curve exhibits a parabolic shape with a minimum at around zero frequency detuning. Also, for the higher applied bias the measured parabola shrank and higher input power requirements were needed to achieve 'normal PS'. In all results included in fig. 7(a) the orthogonally-polarized injected signal was configured with a time duration of 4 ns.

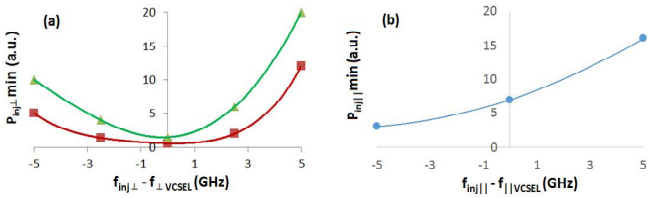

Fig. 7. Experimentally measured maps plotting the minimum injection power vs. frequency detuning for the (a) orthogonally- and (b) parallel-polarized pulsed signals to produce 'normal' and 'reverse' PS. (a) Results are presented for two different values of applied bias current equal to 2.4 mA (red curve) and 4 mA (green curve). (b) The applied bias current and the constant power of the initially injected orthogonally polarized signal were equal to 2.4 mA and 12μW (blue curve). In all cases, the time varying signals injected with orthogonal (a) and parallel (b) polarization had a length of 4 ns.

We have also analyzed theoretically the optimum operating points for the achievement of 'reverse PS' in a 1550nm-VCSEL under DOI. In our calculations we still assumed that the free-running VCSEL emits in its parallel polarization mode. Then, a constant orthogonally polarized optical signal is firstly injected into the VCSEL at a given detuning $\Delta\nu_x$ and with a constant injection power P_{injx} activating the orthogonal polarization and producing 'normal PS'. A pulsed optical signal with parallel polarization is also injected into the device with a frequency detuning $\Delta\nu_y$ and an injection power of P_{injy}. The injection of this second signal switches on the parallel polarization producing 'reverse PS'. Fig. 8(a) shows the calculated map plotting the minimum values of P_{injy} required for 'reverse PS' as a function of the frequency detuning $\Delta\nu_y$ for different values of P_{injx}. The optimum operating point is defined by the vertex of the parabola P_{injy}-$\Delta\nu_y$ which determines the lowest value of injected power required to produce 'reverse PS' ($P_{injy,min}$). This optimal working point is located at negative values of frequency detuning, $\Delta\nu_y$. This result is in good agreement with the corresponding experimental data shown in Fig 7(b). Fig. 7(b) shows for the DOI configuration that the injection strength needed to achieve 'reverse PS' decreases as the detuning crosses zero and reduces towards negative values. Furthermore, fig. 8(a) also shows that the value of $P_{injy,min}$ shifts towards larger negative detuning as the strength of the constant orthogonally-polarized injected power (P_{injx}) is increased. Figs. 8(b) and 8(c) show in detail the evolution of $P_{injy,min}$ as well as the detuning at which it is located, $\Delta\nu_{y,min}$ for increasing values of P_{injx}.

We believe that this displacement towards negative frequency detunings of the minimum injection strength to

This article has been accepted for publication in a future issue of this journal, but has not been fully edited. Content may change prior to final publication. Citation information: DOI 10.1109/JSTQE.2015.2413955, IEEE Journal of Selected Topics in Quantum Electronics

produce 'reverse PS' is due to frequency pushing effects arising in the VCSEL when the device is subject to DOI. The initial injection of the constant optical signal with orthogonal polarization pushes the VCSEL's cavity resonance towards lower frequencies. As a consequence, the minimum injection strength for the second time-varying parallel polarized signal to produce 'reverse PS' will not occur at around zero detuning but will be displaced towards negative values. Besides, the higher the injection strength of the constant orthogonally polarized signal (P_{injx}) the more the VCSEL's cavity resonance is displaced towards lower frequencies and as a result the more the optimal point for 'reverse PS' shifts towards negative frequency detunings.

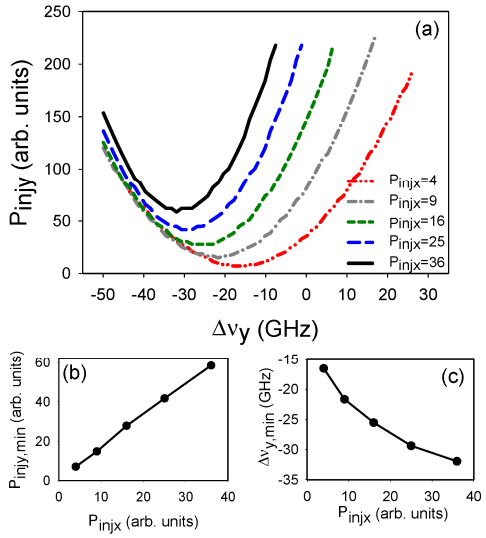

Fig. 8. (color online) (a) Calculated map plotting the minimum injected power for the parallel polarized pulsed signal (P_{injy}) to produce 'reverse PS vs. frequency detuning, $\Delta\nu_y$. Maps have been calculated for several values of the constant orthogonally-polarized optical signal, P_{injx}, which was injected at zero detuning, $\Delta\nu_x = 0$. Evolution of the calculated minimum injected power $P_{injy,min}$ (b) and minimum detuning $\Delta\nu_{y,min}$ for the parallel polarized signal to produce 'reverse PS' as a function of the P_{injx}. The time duration for the pulsed parallel polarized signal was equal to τ_y = 4ns and the normalized bias current was μ = 2.6.

We must also note that the curves calculated in fig. 8(a), independently of the value of P_{injx} configured, show a very similar (different) evolution in their lower (higher) frequency side. This non-uniform shift of the calculated P_{injy}-$\Delta\nu_y$ parabolas is related to the frequency asymmetry introduced by the VCSEL's linewidth enhancement factor, α. In order to further analyze this point we have numerically investigated the effect of α in the optimum operation point for 'reverse PS'.

Fig. 9 plots calculated results for increasing values of α from 0 to 3 and for different values of P_{injx}. Specifically, fig. 9(a) plots calculated results when $\alpha = 0$ showing for this first case the achievement of symmetrical parabolae with minimum values of P_{injy} ($P_{injy,min}$) at zero detuning for all values of P_{injx} considered. Figs. 9(b-d) plotting calculated results for increasing positive values of α from 1 to 3 reveal a higher shift of $P_{injy,min}$ towards negative values of frequency detuning and a larger asymmetry in the calculated parabolae in the P_{injy}-$\Delta\nu_y$ plane as α increases. This larger displacement of the parabolas for higher positive values of alpha ultimately explains the merging of the different P_{injy} curves at the negative side of the detuning $\Delta\nu_y$, also observed in fig. 8(a).

For clarity fig. 10 plots the evolution of the vertex of the parabolas calculated in figs. 9(a-d). Fig. 10 shows that $\Delta\nu_{y,min}$ does not shift towards negative detuning for $\alpha = 0$ (solid-gray line) as P_{injx} increases. However, for increasing values of α significant displacements can be observed in the location of the minimum detuning $\Delta\nu_{y,min}$ as P_{injx} grows.

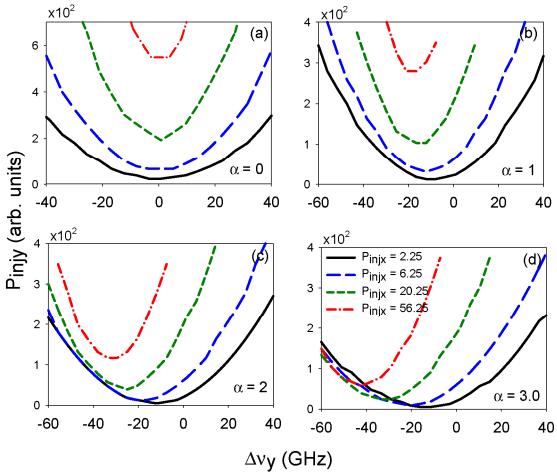

Fig. 9 Calculated map plotting the minimum injected power for the parallel polarized pulsed signals to produce 'reverse PS vs. detuning for different values of the constant injected orthogonal power, P_{injx}. The other parameters are: $\mu = 2.6$, $\Delta\nu_x = 0$ GHz (a) $\alpha = 0$, (b) $\alpha = 1$, (c) $\alpha = 2$ and (d) $\alpha = 3$.

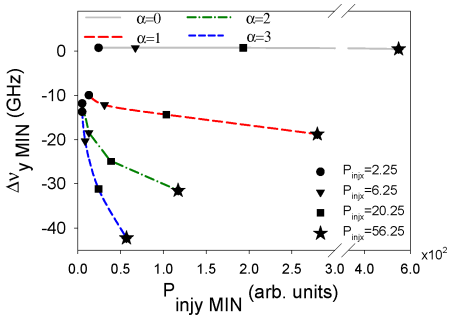

Fig. 10. (color online) Minimum frequency detuning $\Delta\nu_{y,min}$ vs. minimum injected power $P_{injy,min}$ for different values of P_{injx} and α as indicated.

We have also analyzed the influence of the normalized bias current in the DOI configuration. Fig. 11(a) shows calculated maps for different values of normalized bias current μ plotting as a function of $\Delta\nu_y$ the minimum value of P_{injy} required for the achievement of 'reverse PS'. In all cases analyzed in fig. 11(a) the constant injected orthogonally-polarized power was fixed to P_{injx} = 1 arb. units. This value of P_{injx} is already large enough to shift significantly the calculated parabolas towards negative values of frequency detunings (as in fig. 8(a)). Fig. 11(a) also shows that an increase of the normalized bias current μ produces a horizontal shift of the vertices of the parabola. This offset of the optimal point for 'reverse PS' for increasing μ occurs now in the opposite direction to that obtained for increasing values of P_{injx} (see fig. 8(a)). Now,

This article has been accepted for publication in a future issue of this journal, but has not been fully edited. Content may change prior to final publication. Citation information: DOI 10.1109/JSTQE.2015.2413955, IEEE Journal of Selected Topics in Quantum Electronics

with increasing values of μ, $\Delta\nu_{y,min}$ moves towards positive frequency detuning values closer to zero whereas $P_{injy,min}$ remains unchanged. This behaviour can be better seen in figs. 11(b) and 11(c) plotting the evolution of $\Delta\nu_{y,min}$ and $P_{injy,min}$ as functions of μ. As a result, the optimal working point for 'reverse PS' ($P_{injy,min}$, $\Delta\nu_{y,min}$) in a 1550 nm-VCSEL in the DOI configuration can by highly and effectively tuned in the P_{injy}-$\Delta\nu_y$ plane just by controlling the values of two system parameters such as P_{injx} and μ. This large degree of controllability could be effectively used to tune and optimize the operation of VCSEL-based systems utilizing PS for polarization sensitive applications, such as the recently reported all-optical inverter elements [29][30] and novel photonic neurons [36][37] amongst others.

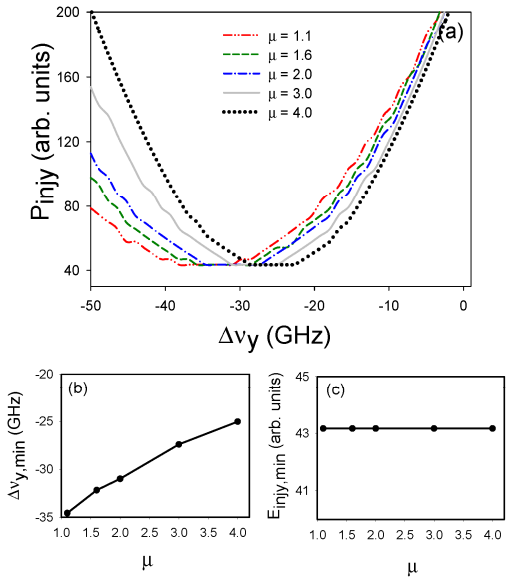

Fig. 11. (color online) (a) Calculated maps plotting the minimum injected power for the parallel polarized pulsed signals to produce 'reverse PS vs. detuning for different values of normalized bias current. Calculated values for the minimum (b) frequency detuning $\Delta\nu_{y,min}$ and (c) injection power $P_{injy,min}$ needed to achieve 'Reverse PS' as a function of the normalized bias current, μ. (P_{injy} = 1 arb. units, $\Delta\nu_y$ = 0 GHz and τ_y = 4ns, α = 2.2).

VI. Conclusions

In this work we have investigated experimentally and in theory the 'normal' and 'reverse' Polarization Switching (PS) obtained in a 1550nm-VCSELs under single (SOI) and double optical injection (DOI). Experimental confirmation is provided for the speed operation enhancement predicted for 'reverse' PS under DOI [30]. Also, we have investigated numerically and experimentally the optimal operating points for 'normal' and 'reverse' PS showing significant differences for the two cases of polarized optical injection analysed. Overall good agreement between theory and experiments is found.

Furthermore, we have numerically characterized the minimal injection power required to obtain both types of PS. We have also determined the influence of important system parameters such as the applied bias current, linewidth enhancement factor, frequency detuning and injection powers in the achievement of 'normal' and 'reverse PS'. We have also identified the variables that modify the optimal operating point for the novel case of 'reverse PS' under DOI.

These results obtained with off-the-shelf and inexpensive devices operating at the important telecom wavelength of 1550nm offer exciting prospects for novel applications of VCSELs in polarization sensitive applications with enhanced operation speed.

References

[1] R. Michalzik, "VCSELs: fundamentals, technology and applications of vertical-cavity surface-emitting lasers," Springer Series in Optical Sciences, vol. 166, Springer-Verlag, Berlin Heidelberg 2013.

[2] F. Koyama, "Recent advances of VCSEL photonics," *J. Lightwave Technol.*, vol. 24, no. 12, pp. 4502-4513, Dec. 2006.

[3] K. Panajotov, M. Sciamanna, I. Gatare, M. Arteaga and H. Thienpont, "Nonlinear dynamics of vertical-cavity surface-emitting lasers," *Advances in Optical Technologies*, vol. 2011, pp. 469627-1 – 46927-16, Jul. 2011.

[4] M. Sciamanna, A. Valle, P. Mégret, M. Blondel and K. Panajotov, "Nonlinear polarization dynamics in directly modulated vertical-cavity surface-emitting lasers," *Phys. Rev. E*, vol. 68, 016207, July 2003.

[5] C. Masoller and M. S. Torre, "Modeling thermal effects and polarization competition in vertical-cavity surface-emitting lasers," *Optics Express*, vol. 16, no. 26, pp. 21282–21296, Dec. 2008.

[6] N.A. Khan, K. Schires, A. Hurtado, I.D. Henning and M.J. Adams, "Temperature dependent dynamics in a 1550-nm VCSEL subject to polarized optical injection," *IEEE J. Quant. Electron.*, vol. 48, no. 5, pp. 712–719, May. 2012.

[7] M. S. Torre and C. Masoller, "Influence of optical feedback on the polarization switching of vertical-cavity surface-emitting lasers," *IEEE J. Quantum Electronics.*, vol. 41, no. 4, pp. 483-489, Apr. 2005.

[8] K. Panajotov, M. Sciamanna, M. Arizaleta-Arteaga and H. Thienpont, "Optical feedback in vertical-cavity surface-emitting lasers," *IEEE J. Select. Topics in Quant. Electron.*, vol. 19, no. 9, 1700312, Jul./Aug. 2013.

[9] Z. G. Pan, S. Jiang, M. Dagenais, R. A. Morgan, K. Kojima, M. T. Asom, R. E. Leibenguth, G. D. Guth and M. W. Focht, "Optical injection induced polarization bistability in vertical-cavity surface emitting lasers," *Appl. Phys. Lett.*, vol. 63, no. 22, pp. 2999–3001, Nov. 1993.

[10] Y. Hong, K. A. Shore, A. Larsson, M. Ghisoni and J. Halonen, "Polarisation switching in a vertical cavity surface emitting semiconductor laser by frequency detuning," *IEEE Proc. Optoelectron.*, vol. 148, no. 1, pp. 31–34, Feb. 2001.

[11] S. Bandyopadhyay, Y. Hong, P.S. Spencer and K.A. Shore, "VCSEL polarization control by optical injection," *J. Lightwave Technol.*, vol. 21, no. 10, pp. 2395-2404, Oct. 2003.

[12] A. Hurtado, A. Quirce, A. Valle, L. Pesquera and M.J. Adams, "Nonlinear dynamics induced by parallel and orthogonal optical injection in 1550 nm Vertical-Cavity Surface-Emitting Lasers (VCSELs)," *Opt. Express*, vol. 18, no. 9, pp. 9423-9428, Apr. 2010.

[13] R. Al-Seyab, K. Schires, A. Hurtado, I.D. Henning and M.J. Adams, "Dynamics of VCSELs subject to optical injection of arbitrary polarization," *IEEE J. Sel. Top in Quantum Electron.*, vol. 19, no. 4, 1700512, July/August 2013.

[14] A. Hurtado, I.D. Henning and M.J. Adams, "Dynamics of polarization switching in 1550nm-VCSELs under single and double optical injection," in *Proc. of SPIE*, vol. 8255, pp. 82550A-1-8, 2012.

[15] M. Torre, A. Hurtado, A. Quirce, A. Valle, L. Pesquera and M. Adams, "Polarization switching in long-wavelength VCSELs subject to orthogonal optical injection," *IEEE J. Quant. Electron.*, vol. 47, no. 1, pp. 92–98, Jan. 2011.

[16] A. Quirce, J. R. Cuesta, A. Valle, A. Hurtado, L. Pesquera and M. Adams, "Polarization bistability induced by orthogonal optical injection in 1550-nm multimode VCSELs," *IEEE J. Select. Topics Quantum Electron.*, vol. 18, no. 2, pp. 772–777, Apr. 2012.

[17] I. Gatare, K. Panajotov and M. Sciamanna, "Frequency-induced polarization bistability in vertical-cavity surface-emitting lasers with

orthogonal optical injection," *Phys. Rev. A*, vol. 75, no. 2, 023804, Feb. 2007.

[18] R. Al-Seyab, K. Schires, N.A. Khan, A. Hurtado, I.D. Henning and M.J. Adams, "Dynamics of polarized optical injection in 1550-nm VCSELs: theory and experiments," *IEEE J. Select. Topics Quantum Electron.*, vol. 17, no. 5, pp.1242-1249, Sep./Oct. 2011.

[19] M. S. Torre and C. Masoller, "Dynamical hysteresis and thermal effects in vertical-cavity surface-emitting lasers," *IEEE J. Quant. Electron.*, vol. 46, no. 12, pp. 1788-1794, Dec. 2010.

[20] Y. Hong, C. Masoller, M.S. Torre, S. Priyadarshi, A.A. Qader, P.S. Spencer and K. Shore, "Thermal effects and dynamical hysteresis in the turn-on and turn-off of vertical-cavity surface-emitting lasers," *Opt. Lett.*, vol. 35, no. 21, pp. 3688-3690, Nov. 2010.

[21] A.A. Qader, Y. Hong and K.A. Shore, "Ultra-wide hysteresis frequency bistability in vertical cavity surface emitting lasers subject to orthogonal optical injection," *Appl. Phys. Lett*. 103, 021108, Jul. 2013.

[22] A. Quirce, A. Valle and L. Pesquera, "Very wide hysteresis cycles in 1550-nm VCSELs subject to orthogonal optical injection," *IEEE Phot. Tech. Lett.*, vol. 21, no. 17, pp. 1193-1195, Sep. 2009.

[23] A. Hurtado, A. Quirce, A. Valle, L. Pesquera and M. J. Adams, "Power and wavelength polarization bistability with very wide hysteresis cycles in a 1550nm-VCSEL subject to orthogonal optical injection," *Opt. Express*, vol. 17, no. 26, pp. 23637-23642, Dec. 2009.

[24] M.F. Salvide, C. Masoller and M.S. Torre, "Polarization switching and hysteresis in vertical-cavity surface-emitting lasers subject to orthogonal optical injection," *IEEE J. Quant. Electron.*, vol. 50, no. 10, pp. 848-853, Oct. 2014.

[25] J. Sakaguchi, T. Katayama and H. Kawaguchi, "High switching-speed operation of optical memory based on polarization bistable vertical-cavity surface-emitting laser," *IEEE J. Quant. Electron.*, vol. 46, no. 11, pp. 1526–1534, Nov. 2010.

[26] J. Sakaguchi, T. Katayama and H. Kawaguchi, "All-optical memory operation of 980-nm polarization bistable VCSEL for 20-Gb/s PRBS RZ and 40-Gb/s NRZ data signals," *Opt. Exp.*, vol. 18, no. 12, pp. 12362–12370, Jun. 2010.

[27] S. H. Lee, H. W. Jung, K. H. Kim, M. H. Lee, B. S. Yoo, J. Roh and K. A. Shore, "1-GHz all-optical flip-flop operation of conventional cylindrical-shaped single-mode VCSELs under low-power optical injection," *IEEE Photon. Technol. Lett.*, vol. 22, no. 23, pp. 1759–1761, Dec. 2010.

[28] S. H. Lee, H. W. Jung, K. H. Kim and M. H. Lee, "All-optical flip-flop operation based on polarization bistability of conventional 1.55-μm wavelength single-mode VCSELs," *J. Opt. Soc. Korea*, vol. 14, no. 2, pp. 137–141, Jun. 2010.

[29] A. Quirce, J. R. Cuesta, A. Hurtado, K. Schires, A. Valle, L. Pesquera, I. D. Henning and M. J.Adams, "Dynamic characteristics of an all-optical inverter based on polarization switching in long-wavelength VCSELs," *IEEE J. Quant. Electron.*, vol. 48, no. 5, pp. 588-595, May. 2012.

[30] P. Pérez, A. Valle, L. Pesquera and A. Quince, "All-optical inverter based on polarization switching in VCSELs subject to single and dual optical injection," *IEEE J. Sel. Topics in Quant. Electron.*, vol. 19, no. 4, 1700408, Jul./Aug. 2013.

[31] T. Mori, Y. Sato and H. Kawaguchi, "Timing jitter reduction by all-optical signal regeneration using a polarization bistable VCSEL," *J. Lightwave Technol*., vol. 26, no. 16, pp. 2946-2953, Aug. 2008.

[32] A. Quirce, P. Pérez, H. Lin, A. Valle, L. Pesquera, K. Panajotov and H. Thienpont , "Polarization switching regions of optically injected long-wavelength VCSELs," *IEEE J. Quant. Electron.*, vol. 50, no. 11, pp. 921-928, Sept. 2014.

[33] V.M. Deshmukh, S. H. Lee, D. W. Kim, K. H. Kim and M. H. Lee, "Experimental and numerical analysis on temporal dynamics of polarization switching in an injection-locked 1.55-µm wavelength VCSEL," Opt. Express, vol. 19, no. 18, pp. 16934-16949, Aug. 2011.

[34] M. Salvide, C. Masoller and M. S. Torre, "All-optical stochastic logic gate based on a VCSEL with tunable optical injection," *IEEE J. Quant. Electron.*, vol. 49, no. 10, pp. 863-893, Oct. 2013.

[35] S. Perrone, R. Vilaseca and C. Masoller, "Stochastic logic gate that exploits noise and polarization bistability in an optically injected VCSEL," *Opt. Exp.*, vol. 20, no. 20, pp. 22692–22699, Sep. 2012.

[36] A. Hurtado, K. Schires, I. D. Henning and M. J. Adams, "Investigation of vertical cavity surface emitting laser dynamics for neuromorphic photonic systems," *Appl. Phys. Lett.*, vol. 100, 103703, Mar. 2012.

[37] A. Hurtado, I. D. Henning and M. J. Adams, "Optical neuron using polarisation switching in a 1550nm-VCSEL," *Opt. Exp.*, vol. 18, no. 24, pp. 25170-25176, Nov. 2010.

[38] M.-R. Park, O.-Kyun Kwon, W.-S. Han, K.-H. Lee, S.-J. Park and B.-S. Yoo, "All-monolithic 1.55µm InAlGaAs/InP vertical cavity surface emitting lasers grown by metal organic chemical vapor deposition," *Jpn. J. Appl. Phys*. vol. 45, L8–L10 (2006).

[39] J.M. Martín-Regalado, F. Prati, M. San Miguel and N.B. Abraham, "Polarization properties of vertical cavity surface-emitting lasers," *IEEE J. Quantum Electron.*, vol. 33, no. 5, pp. 765-783, May. 1997.

[40] P.E. Kloeden and E. Platen, "Numerical solution of stochastic differential equations," Applications of Mathematics, vol. 23, Springer-Verlag, Berlin, 1992.

[41] E.K. Lau, L.J. Wong and M.C. Wu, "Enhanced modulation characteristics of optical injection-locked lasers: A tutorial," *IEEE J. Select. Topics Quantum Electron.*, vol. 15, no. 3, pp. 618-633, May/June 2009.

[42] X. Wang and L. Chrostowski, "High-speed Q-modulation of injection-locked semiconductor lasers," *IEEE Photon. J.*, vol. 3, no.5, pp. 936-945, Oct. 2011.

[43] A. A. Qader, Y. Hong and K. A. Shore, "Role of suppressed mode in the polarization switching characteristics of optically injected VCSELs," *IEEE J. Quantum Electron.*, vol. 49, no. 2, pp. 205-210, Feb. 2013.

Antonio Hurtado received his PhD degree in Telecommunications Engineering from the Universidad Politécnica de Madrid (Spain) in 2006. In 2007 he joined the Optoelectronics Research Group at the University of Essex (UK) and from 2011 to 2013 he worked at the Centre for High Technology Materials, University of New Mexico (USA). He has been awarded two consecutive Marie Curie Fellowships by the European Commission. In 2014 he was appointed as Lecturer (Strathclyde Chancellor's Fellowship) in the Strathclyde's Institute of Photonics.

Ian D. Henning received the degree in applied physics and the Ph.D. degree from the University of Wales, Cardiff, U.K. In 1980, he joined British Telecom Research Laboratories at Martlesham Heath, working on the design and characterisation of a range of optoelectronic devices and photonic integrated circuits. In 2002 he joined University of Essex, Colchester, U.K as a Professor.

Michael J. Adams received the Ph.D. degree in laser theory from the University of Wales, Cardiff, U.K., in 1970. He was engaged in optoelectronics research and development with 15 years of experience in industry (Plessey, BT), and 29 years of experience in academia (University of Cardiff, University of Southampton, University of Essex, Colchester, U.K.). Since 1996 he has been a Professor at the University of Essex.

Matias F. Salvide received the Licenciado en Física (Ms. Sc.) degree from the Universidad Nacional del Centro de la Provincia de Buenos Aires (UNCPBA), Buenos Aires, Argentina, in 2012. He is currently working toward the PhD degree in Physics. His current research interests are in the areas of dynamics of vertical-cavity surface-emitting lasers and optical injection effects in semiconductor lasers.

M. S. Torre received the Ph. D. degree from the Universidad Nacional del Centro de la Provincia de Buenos Aires (UNCPBA), Buenos Aires, Argentina. She is currently a Research Professor at the Facultad de Ciencias Exactas of the UNCPBA and Independent Researcher CONICET (National Council of Scientific and Technical Investigations.